Analysis of 3*d* photoionization and subsequent Auger decay of atomic germanium

K. Jänkälä,[1,*] D. Anin,[1] S. Urpelainen,[1,2] S.-M. Huttula,[1] S. Heinäsmäki,[1] and M. Huttula[1]
[1]*Department of Physical Sciences, P.O. Box 3000, University of Oulu, FI-90014 Oulu, Finland*
[2]*MAX-lab, Lund University, Box 118, SE-22100 Lund, Sweden*
(Received 16 September 2011; published 3 November 2011)

Experimental and theoretical study of the 3*d* photoionization and subsequent Auger decay of initially neutral atomic germanium is presented. The features of the high-resolution photoelectron and Auger electron spectra are interpreted with the aid of multiconfiguration calculations. The binding energies and relative cross sections of the 3*d* ionized fine-structure states of Ge are given. The complete $M_{4,5}NN$ Auger electron spectrum to doubly ionized final states of the Ge ion is interpreted and discussed.

DOI: 10.1103/PhysRevA.84.052501 PACS number(s): 32.10.−f, 32.80.Fb, 32.80.Hd, 31.15.A−

I. INTRODUCTION

Germanium is one of the most important elements in the present semiconductor technology. Its uses range also to, for example, optical devices and solar cells, and it acts as a catalyst in different chemical reactions. During recent years numerous studies of pure and mixed germanium clusters have been published (see, e.g., Refs. [1–3] and references therein). When germanium atoms bond together, the valence 4*s* and 4*p* orbitals hybridize and form delocalized electronic bands. Therefore, 3*d* is the first orbital that remains localized in the solid and clusterized Ge. The properties of the 3*d* orbital can thus be used to effectively probe the chemical environment in the surface of solid Ge (see, e.g., Refs. [4,5]) or in clusters. The 3*d* ionization has been also recently used as as tool to study Ge nanowires [6].

Despite of wide range of studies of Ge in compounds, films, and solids, in addition to the optical data listed in Ref. [7] and radiative lifetimes of the valence-excited Ge [8], only a few studies of atomic Ge have been published. Aksela and Aksela published the electron-impact-induced $L_{2,3}MM$ Auger electron spectrum (AES) of atomic Ge [9] and more recently Kovalik *et al*. studied the KLL AES of Ge [10]. The electron impact ionization cross section of atomic Ge was studied experimentally in Ref. [11] and theoretically in Ref. [12]. To our knowledge, no prior studies of 3*d* photoionization and the following Auger decay of initially neutral atomic Ge exist.

In this paper we provide an experimental and theoretical investigation of the 3*d* photoionization and subsequent Auger decay of atomic germanium. The paper continues our efforts in providing fundamental spectroscopic information (binding energies, ionization cross sections, coupling conditions, etc.) for the inner shell ionization of industrially important high-evaporation-temperature metals and semimetals in atomic form. These studies were recently conducted by our group for Al [13] and for the Group 14 elements Si [14], Sn [15], and Pb [16]. The reported measurement on 3*d* ionization of Ge thus completes the series on Group 14 metals.

The paper is structured as follows. The experimental setup and the theoretical methods are described in Secs. II and III. The results in Sec. IV are presented by first describing the 3*d* ionized fine-structure states of Ge and the 3*d* photoelectron spectrum (PES), which is followed by a brief description of the subsequent Auger decay. We conclude with a summary.

II. EXPERIMENT

The experiment was carried out at the 1.5 GeV MAX-II synchrotron radiation source (Lund, Sweden) at the undulator beam line I411 [17]. The electron spectra were measured using a Scienta R4000 hemispherical electron energy analyzer. In order to obtain relative intensities directly proportional to the angle-integrated cross sections, the electron spectra were measured at the "magic" angle of 54.7°, with respect to the polarization vector of the linearly polarized synchrotron radiation. The beam of atomic Ge at a temperature of 1300 °C was produced by using an inductively heated oven system (for a detailed description, see Ref. [18]). At a temperature of approximately 1300 °C, three thermally excited states are considerably populated in the Ge vapor, namely $[\mathrm{Ar}]3d^{10}3s^23p^2\,{}^3P_{0,1,2}$ triplet states. The population of the states was estimated using the Boltzmann distribution with the energy separations from the NIST database [7]. The estimation gives populations 24%, 43%, and 33% for the ${}^3P_0$, ${}^3P_1$, and ${}^3P_2$ initial states, respectively. At temperatures needed to evaporate Ge, the Boltzmann distribution is a slowly varying function. Therefore, all practical evaporation temperatures yield this initial state distribution with only minor changes.

The photoelectron and Auger electron spectra were measured at a photon energy of 113 eV. The experimental broadening for the PES was about 50 meV and for the AES about 40 meV. A 1-mm-diam- hole in the hat of the oven crucible partially collimated the Ge vapor beam, which reduced the Doppler broadening to be small compared to other broadening factors. The binding energy scale for PES was calibrated using the Xe 4*d* photoelectron lines [19], whereas the kinetic energy for AES was calibrated using the Xe $N_{4,5}O_{2,3}O_{2,3}$ Auger electron lines. The transmission function of the analyzer was determined experimentally using the constant ratio between the Xe 4*d* photoelectron and Auger electron lines as described in Ref. [20].

III. THEORY AND CALCULATIONS

The calculations were carried out using the multiconfiguration Dirac-Fock (MCDF) method by applying the GRASP92 and GRASP2K codes [21,22] together with the RELCI extension [23].

*kari.jankala@oulu.fi

The MCDF method is described in detail elsewhere (see, e.g., Ref. [21] and references therein). Therefore, only the main principles are reviewed here. In the MCDF method, the atomic state functions (ASFs), characterized by the total angular momentum J_α and parity P_α, are represented in the basis of jj-coupled configuration state functions (CSFs) with the same J_α and P_α

$$|\Psi_\alpha(P_\alpha J_\alpha)\rangle = \sum_k c_{\alpha k}|\psi_k(P_\alpha J_\alpha)\rangle. \quad (1)$$

The mixing coefficients $c_{\alpha k}$ are obtained by diagonalizing the two-electron interaction matrix which allows to take the electronic correlations into account. The wave functions are obtained self-consistently using the Dirac-Coulomb Hamiltonian.

Because of the light mass of Ge, the orbital and spin angular momenta of the outer electrons are not strongly interacting. Therefore, the coupling conditions are closer to the LSJ coupling. Thus for the analysis the inherently jj-coupled ASFs were transformed into the LSJ basis by the unitary transform between the two bases applying the program LSJ [24].

The photoionization cross sections [25] were computed by performing separate MCDF calculations for the initial and final ionic states, and then coupling an energy-normalized continuum wave function to the latter. Using the relativistic form of the electric dipole interaction operator results in the differential cross-section formula

$$\frac{d\sigma}{d\Omega} = \frac{4\pi^2}{3(2J_0+1)\alpha\omega} \times \sum_{Jlj}\int d\epsilon \left|\langle\alpha_0 J_0||\sum_{i=1}^{N_e}\boldsymbol{\alpha}_i\cdot\boldsymbol{e}||\alpha_\beta J_\beta,(\epsilon lj);J\rangle\right|^2, \quad (2)$$

where the operator $\boldsymbol{\alpha}$ stems from the Dirac equation [26] and $\boldsymbol{e}$ is the polarization vector of the synchrotron radiation. We have averaged over the initial and summed over the final magnetic substates and used the Wigner-Eckart theorem. When computing the matrix elements in (2) we used an approximation where only the electron undergoing ionization was treated as active and the other orbitals were fixed. This results in a scheme where the many-electron matrix element reduces to one-electron ionization amplitudes multiplied by recoupling coefficients. This approximation takes into account electron correlation effects through configuration interaction and energy dependence of the single-particle ionization amplitudes, but neglects effects arising from overlap matrix elements between orbitals of the same (l,j) symmetry, which are responsible for (shake-type) satellite transitions in addition to small overall scaling of the amplitudes.

The Auger amplitudes were determined by using the AUGER component of the RATIP package [27]. The intensity of the Auger electrons is given by

$$n_{f\beta} = \frac{2\pi\sum_{l_A j_A}\left|\sum_{\mu\nu} c_{f\mu}c_{\beta\nu}M^{\mu\nu}_{f\beta}(J_f,J_\beta)\right|^2}{P_\beta(J_\beta)}Q_\beta(J_\beta), \quad (3)$$

where $M^{\mu\nu}_{f\beta}(J_f,J_\beta)$ is the Coulomb matrix element $\langle\psi_\mu(J_f)\epsilon lj;J_\beta||\sum_{mn}^{N-1}1/r_{mn}||\psi_\nu(J_\beta)\rangle$, $P_\beta(J_\beta)$ is the total decay rate, and $Q_\beta(J_\beta)$ is the $|\Psi(J_0)\rangle \to |\Psi(J_\beta)\rangle$ ionization cross section obtained from (2). For more details about the AUGER program see Refs. [27–29] and references therein.

The experimental spectra are interpreted using single-configuration calculations for the neutral initial and singly ionized intermediate states. The final doubly ionized states are described by a three-configuration calculation. The initial-state configuration $[\mathrm{Ar}]3d^{10}4s^24p^2$ gives five energy levels, from which the three lowest are thermally populated. The configuration $[\mathrm{Ar}]3d^94s^24p^2$ describing the $3d^{-1}$ states couples to 28 fine-structure energy levels. The three configurations $[\mathrm{Ar}]3d^{10}(4s^2,4s4p,4p^2)$ used in the doubly ionized final-state calculation give 10 levels. From these, five levels ($4s^2\,{}^1S_0$, $4s4p\,{}^3P_{0,1,2}$, and $4s4p\,{}^1P_1$) are energetically allowed to be populated via Auger decay. The $4p^2$ configuration is important in predictions due to the Coulomb interaction between the $4s^2$ and $4p^2$ configurations, which shifts the $4s^2\,{}^1S_0$ state to about 1 eV lower in total energy. During the analysis the calculations were extended to include single and double valence excitations to $4d$, $4f$, $5s$, and $5p$ orbitals, but no significant improvement in the energies or in intensities in comparison to the experiment were seen. Therefore, the simplest CSF basis was chosen. All calculations were performed in the average level scheme.

IV. RESULTS AND DISCUSSION

A. 3*d* photoionization of atomic Ge

The experimental and simulated $3d$ PES of atomic Ge are shown in Fig. 1. Due to the presence of three initial states and quite small energy splitting of the fine-structure states of $3d$ ionized Ge, most of the features observed in the spectrum are composed of several overlapping fine-structure lines. This is highlighted in Figs. 1(b)–1(e), where the calculated $3d$ PES from the three initial states and their sum are plotted. However, due to good agreement between the simulated and experimental spectra, the most prominent structures in the experimental spectrum can be identified. The experimental spectrum (dots) in Fig. 1(a) was fitted using Voigt line profiles. The Gaussian width accounting for experimental broadening of all lines is 50 meV and was determined from the valence PES of Xe. The Lorentzian widths arising from the lifetimes of the states were optimized during the fit, so it was set to be the same for peaks 1–22 and individual for peaks 23–29. The Lorentzian width obtained from the fit for lines 1–22 is 39 meV and for lines 23–29 varies in the range 33–49 meV. The result of the fit is depicted in Fig. 1(a) as a solid (red) line corresponding to the sum of all profiles and as vertical (blue) lines corresponding to the height of individual peaks. The peaks and their assignments are listed in Table I. We emphasize that only the dominant transitions according to the calculations are labeled for the fitted peaks. In addition to the lines due to ionization of atomic Ge shown in Fig. 1(a), a structure identified to be caused by $3d$ ionization of small Ge_N clusters was observed at the lower-binding-energy region of about 35–37 eV. For the sake of clarity, the configuration notation $3d^94s^24p^2$ is omitted in the following when appropriate.

The identification and initial placing of the peaks in Fig. 1(a) was done using theoretical calculations by taking the most prominent structures. When possible, the theoretical insight

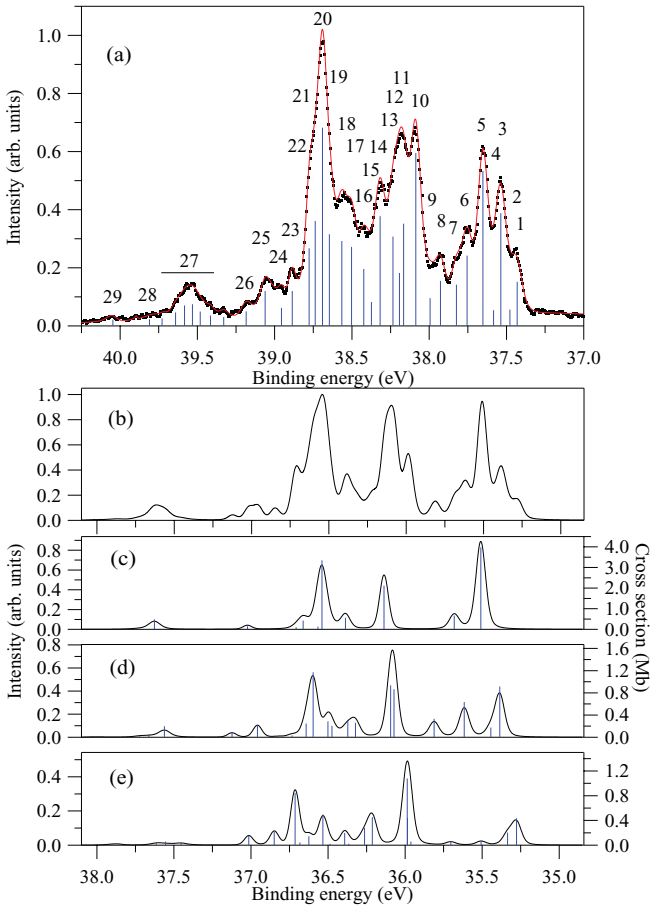

FIG. 1. (Color online) (a) Measured and (b)–(e) simulated 3*d* PES of atomic Ge at the temperature of 1300 °C. The spectrum in (b) is a sum of the spectra from the three initial states $^3P_0$, $^3P_1$, and $^3P_2$ shown in (c)–(e), respectively. The weights of the initial states are obtained from the Boltzmann distribution. The calculated lines are convolved with 60 meV Gaussian and calculated Lorentzian linewidths.

TABLE I. Peak assignments and evaluated binding energies of the most prominent structures seen in the experimental 3*d* PES of atomic Ge in Fig. 1(a). The second and third columns give the initial and final fine-structure states. The $4p^2$ parental coupling of the final states is ^3P unless otherwise stated. The rightmost column gives the intensity percentage of each structure from the total intensity.

Label	Initial	Final	E_b (eV)	Intensity
1	$^3P_2$	$^4D_{7/2}$	37.43(2)	2.2
2	$^3P_2$	$^4D_{5/2}$	37.48(2)	0.8
3	$^3P_1$	$^4D_{7/2}$	37.54(2)	5.7
4	$^3P_1$	$^4D_{5/2}$	37.58(2)	0.8
5	$^3P_0$	$^4D_{5/2}$	37.65(2)	7.8
6	$^3P_1$	$^4D_{3/2}$	37.76(2)	3.5
7	$^3P_0$	$^4D_{3/2}$	37.82(2)	2.1
8	$^3P_1$	$^4D_{1/2}$	37.93(2)	2.3
9	?	?	37.99(2)	1.4
10	$^3P_2$	$^4F_{7/2,9/2}$	38.09(3)	8.7
11	$^3P_1$	$^2F_{5/2}$	38.17(2)	5.2
12	$^3P_1$	$^4F_{7/2}$	38.19(2)	2.7
13	$^3P_0$	$^2F_{5/2}$	38.23(2)	4.5
14	$^3P_2$	$^4P_{5/2}$	38.32(2)	5.5
15	$^3P_2$	$^2D_{3/2}$	38.37(4)	1.2
16	$^3P_1$	$^4P_{5/2}$	38.42(2)	2.9
17	$^3P_{0,1,2}$	$^4P_{5/2}$,$^2D_{3/2}$,$^2P_{3/2}$	38.50(4)	4.0
18	$^3P_{0,1,2}$	$^4P_{5/2}$,$^2D_{3/2}$,$^2P_{3/2}$	38.57(4)	4.3
19	$^3P_1$	$^4F_{3/2}$,$^2P_{3/2}$	38.65(4)	4.6
20	$^3P_{0,2}$	$^4F_{3/2}$,$^4F_{5/2}$	38.69(4)	10.0
21	$^3P_1$	$^2D_{5/2}$	38.74(3)	5.3
22	$^3P_2$	$^2F_{7/2}$	38.78(3)	3.9
23	$^3P_2$	$^4P_{3/2}$	38.89(2)	1.8
24	$^3P_1$	$^4P_{3/2}$	38.96(2)	0.7
25	$^3P_{2,0}$	$^4P_{1/2}$,$^4P_{3/2}$	39.06(3)	0.5
26	$^3P_1$	$^4P_{1/2}$	39.18(2)	0.5
27	$^3P_{0,1}$	$^2P_{3/2}$	39.54(8)	3.9
28	$^3P_{1,2}$	$(^1D)^2D_{3/2}$	39.80(4)	0.3
29	$^3P_{0,1}$	$(^1D)^2F_{5/2}$	40.05(3)	0.3

was combined with experimental knowledge on the energy splitting of the initial states [7]. As an example, according to the calculations, peaks 1 and 3 in Fig. 1(a) arise from photoionization from $^3P_2$ and $^3P_1$ initial states, respectively, to a $^4D_{7/2}$ final state. Identification based on the calculation can be therefore confirmed further by the fact that the observed energy splitting of peaks 1 and 3 is indeed the same as the experimentally known energy difference (106 meV [7]) of the initial states $^3P_2$ and $^3P_1$. This allows fixing the energy difference of the peaks to the known energy difference between the initial states for the fit. In the same fashion, for example, the energy spacing of peaks 5, 4, and 2 was fixed to the energy difference of the initial states (see Table I). We note that, as discussed above, the binding-energy differences and Lorentzian widths of some lines were connected, but otherwise fitting parameters were free, and no values from the calculations were used to fix anything in the fit.

The structures in the experimental 3*d* photoelectron spectrum of atomic Ge depicted in Fig. 1(a) can be identified in *LSJ* coupling as follows. Peaks 1–8 are mainly due to ionization to ^4D_J and peaks 10–13 to $^{2,4}F_J$ final states. Structures labeled as peaks 14–22 are heavily overlapping and the levels are strongly mixed. The leading CSF coefficients of the lines in the region are $^{2,4}F_J$, $^{2,4}P_J$, and ^2D_J. Peaks 23–26 are caused by ionization to high-spin ^4P_J and peak 27 to low-spin ^2P_J states. The small structures 28 and 29 are the only lines seen where the initial ^3P coupling of the $4p^2$ electrons changes to ^1D. More detailed identification of the peaks is given in Table I.

From Table I we find that the dipole-allowed 3*d* photoionization threshold from the $^3P_0$ ground state into the $^4D_{5/2}$ final state is 37.65(2) eV. On the other hand, the first observed photoelectron peak is from the $^3P_2$ initial state into the $^4D_{7/2}$ final state at 37.43(2) eV in binding energy. From this one can calculate that the (dipole-forbidden) 3*d* ionization threshold from the ground state of atomic Ge is 37.61(2) eV. In general the agreement between the experiment and theory on the distribution of line energy positions is quite good. If the experimental and calculated spectra are aligned to peak 1, the calculated spectrum needs to be shifted about 2.15 eV into the lower binding energy. Also, the predicted relative energy (with respect to peak 1) of states at higher binding energy (structures 27–29) tend to spread in energy. These are common problems in configuration-interaction

TABLE II. Calculated and experimental binding energies of $3d$ singly ionized states of atomic Ge. The binding energies are given in eV with respect to the ionization threshold of 37.61(2) eV (experimental) and 35.45 eV (calculated) from the $^3P_0$ ground state. The final-state column shows the LSJ terms of the leading CSF from the $3d^9 4p^2 4s^2$ configuration. The LS term in brackets shows the $4p^2$ parental coupling. The table shows also the calculated $3d$ photoionization cross sections (in Mb) at the photon energy of 113 eV. Column Γ gives the calculated lifetimes (in meV) and the rightmost column gives the purities of states in LSJ coupling.

			Cross section				
Final state	ΔE_b^{expt}	ΔE_b^{calc}	$^3P_0$	$^3P_1$	$^3P_2$	Γ	$\lvert c_1^{LS}\rvert^2$
$(^3P)^4D_{7/2}$	0.00	0.00	0.00	0.91	0.43	25	0.96
$(^3P)^4D_{5/2}$	0.05(2)	0.06	3.98	0.18	0.20	24	0.84
$(^3P)^4D_{3/2}$	0.22(2)	0.23	0.67	0.64	0.07	26	0.85
$(^3P)^4D_{1/2}$	0.39(2)	0.43	0.00	0.33	0.06	26	0.98
$(^3P)^2F_{5/2}$	0.63(2)	0.69	2.11	0.86	0.06	13	0.54
$(^3P)^4F_{7/2}$	0.66(2)	0.71	0.00	0.93	0.43	19	0.73
$(^3P)^4F_{9/2}$	0.66(3)	0.71	0.00	0.00	1.08	24	0.98
$(^3P)^4P_{5/2}$	0.89(2)	0.94	0.56	0.26	0.45	17	0.61
$(^3P)^2D_{3/2}$	0.94(4)	0.99	0.00	0.30	0.28	40	0.46
$(^3P)^4F_{3/2}$	1.11(4)	1.09	3.35	0.20	0.02	40	0.59
$(^3P)^2P_{3/2}$	1.11(4)	1.11	0.13	0.29	0.20	11	0.36
$(^3P)^2D_{5/2}$	1.20(3)	1.21	0.43	1.17	0.02	22	0.32
$(^3P)^4F_{5/2}$		1.26	0.10	0.25	0.50	18	0.30
$(^3P)^2P_{1/2}$		1.35	0.00	0.03	0.15	9	0.57
$(^1D)^2S_{1/2}$		1.41	0.00	0.00	0.04	42	0.75
$(^3P)^2F_{7/2}$	1.35(3)	1.44	0.00	0.01	0.85	10	0.73
$(^3P)^4P_{3/2}$	1.46(2)	1.57	0.15	0.22	0.22	12	0.62
$(^1D)^2G_{9/2}$		1.66	0.00	0.00	0.00	23	0.98
$(^3P)^4P_{1/2}$	1.65(2)	1.74	0.00	0.08	0.15	12	0.64
$(^1D)^2G_{7/2}$		2.09	0.00	0.00	0.00	21	0.81
$(^3P)^2P_{3/2}$	1.99(8)	2.18	0.49	0.20	0.04	51	0.43
$(^1D)^2D_{5/2}$		2.28	0.05	0.05	0.06	110	0.71
$(^1D)^2P_{1/2}$		2.34	0.00	0.02	0.03	44	0.70
$(^1D)^2F_{7/2}$		2.58	0.00	0.00	0.01	9	0.81
$(^1D)^2D_{3/2}$	2.37(4)	2.62	0.00	0.01	0.03	78	0.69
$(^1D)^2F_{5/2}$	2.44(3)	2.96	0.01	0.01	0.00	13	0.91
$(^1S)^2D_{5/2}$		4.16	0.00	0.00	0.00	18	0.89
$(^1S)^2D_{3/2}$		4.70	0.00	0.00	0.00	18	0.92

methods and are due to missing correlations and overestimated exchange interaction. The discrepancies may be corrected by increasing the size of the CSF space considerably, which is, however, out of the scope of this paper.

Table II shows the calculated binding energies, photoionization cross sections at the photon energy of 113 eV, lifetimes, and purities in LSJ coupling of all of the 28 $[\text{Ar}]3d^9 4s^2 4p^{2(2S+1)}L_J$ fine-structure states of Ge^+. Table II gives also the experimentally obtainable energy comb of the $Ge^+(3d^{-1})$ fine-structure states isolated from Table I. We find from Table II that the total energy spreading of the $Ge^+(3d^{-1})$ fine-structure array is about 4.7 eV and the states are quite well described in LSJ coupling so that the average purity of the states is about 0.7.

Even though Hund's rules cannot be blindly applied to correlated three-electron (or hole) cases [30], Hund's rule ordering is well seen in the parental coupling of the $4p^2$ electrons. The high-spin $4p^2\,^3P$ coupled states lay clearly in the lower binding (total) energy and the low-spin ^1D and ^1S states in the higher binding energy, so that the states with the smallest orbital angular momenta have the highest binding energy. The parental $4p^2$ coupling gives thus a fairly good quantum number and the coarse energy ordering of the fine-structure states can be understood by looking at the Coulomb interaction between the outermost $4p$ electrons. The stability of the $4p^2$ coupling is even more evident if one considers the photoionization cross sections. The ionization probabilities to the final ionic states having the ^1S or ^1D singlet $4p^2$ parental coupling are negligibly small. This is due to the fact that single electron ionization from the $3d$ orbital does not change the $4p^2$ coupling. Therefore, the only way to obtain a nonzero cross section from the pure triplet initial state to the singlet $4p^2$ coupled final state is via configuration interaction.

The spin-orbit interaction defines the spectral structures observed in the $3d$ PES of solid Ge [4,6]. This is understood assuming that the delocalized valence electrons do not interact strongly with the $3d$ hole in the solid. In atomic Ge the two $4p$ electrons are present, and the spin-orbit interaction of the $3d$ hole is less evident. If one, however, looks at the $3d$ ionized states of atomic Ge in the jj-coupled basis, the states having the leading CSF coefficient with $3d_{5/2}$ parent coupling are in general found at smaller binding energies and the $3d_{3/2}$ states at higher binding energies.

One may compare the $3d$ ionized states of Ge also to the Group 14 neighboring elements, namely $2p$ ionized states of Si [14] and $4d$ ionized states of Sn [15]. Comparison shows that the two valence $4p$ electrons are more independent in Ge than the two $3p$ valence electrons in Si, since in $2p$ ionization of Si several lines with changing $3p^2$ parental coupling were seen. In addition, the parental coupling of the $3p^2$ electrons in Si follows Hund's rules less strictly. On the other hand, comparison to Sn shows that increasing strength of the spin-orbit interaction affects more the energy ordering of the $4d$ ionized states of Sn.

B. $M_{4,5}NN$ Auger decay of atomic Ge

The experimental and calculated AES resulting from the Auger decay of $3d$ ionized states of atomic Ge are depicted in Fig. 2. The five energetically allowed doubly ionized final states are $4s^2\,^1S_0$, $4s4p\,^3P_{0,1,2}$, and $4s4p\,^1P_1$. The mean kinetic energies of the Auger electron groups and their intensity branching ratios are given in Table III. The $M_{4,5}NN$ Auger electron lines lay at small kinetic energies, which are difficult to study reliably with hemispherical electron energy analyzers. The spectrum presented in Fig. 2(a) is transmission corrected, but especially the analysis of the intensities of the Auger electron lines corresponding to the $4s4p\,^1P_1$ final state is hampered by badly behaving transmission. In the present the scope is to provide only a tentative description for the observed spectral structures.

The kinetic energies of the groups of Auger electron lines are well predicted. Especially the kinetic energy positions of the $4s4p\,^3P_{0,1,2}$ and $4s^2\,^1S_0$ final states agree remarkably well with the experimental values. The $4s4p\,^1P_1$ group is found at slightly higher kinetic energies than predicted. This is at least partly due to missing electron correlation, since the calculation with the larger CSF basis including double valence

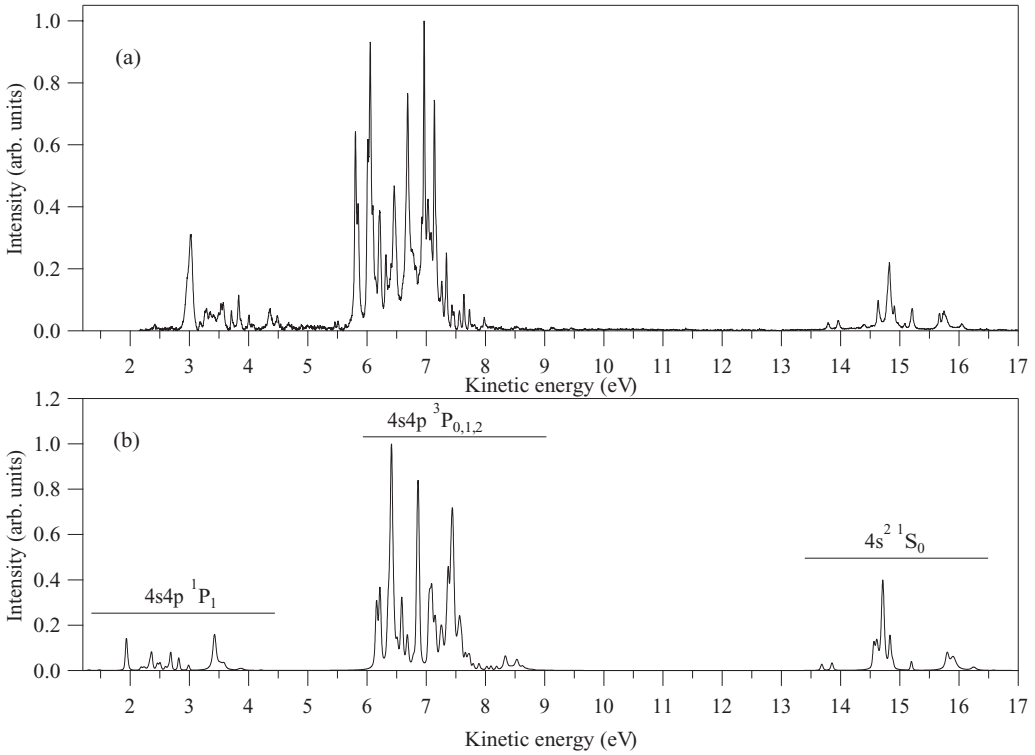

FIG. 2. (a) Experimental and (b) calculated Auger electron spectrum following the 3*d* ionization of atomic Ge at a temperature of 1300 °C.

excitations to $4d$, $4f$, $5s$, and $5p$ orbitals, shifts the kinetic energy of the group about 100 meV. This indicates that better energy positions may be calculated, but that would require a considerably larger CSF basis than the presently used.

One sees immediately from Fig. 2(a) that the final-state group $4s4p\,^3P_{0,1,2}$ is the favored decay channel. The main reason for this is obviously that, in the group, the three final states are overlapping. The states are separated by 90 meV ($^3P_1$) and 300 meV ($^3P_2$) from the $^3P_0$ state. According to the calculations, the branching ratios of the calculated individual $4s4p\,^3P_{0,1,2}$ final states are 0.35 ($^3P_2$), 0.32 ($^3P_1$), and 0.09 ($^3P_0$). This shows that in the 3*d* Auger decay, the decay probability to, for example, $4s4p\,^3P_1$, is about twice the probability for the decay to the $4s4p\,^1P_1$ final state.

The shapes of the three individual structures are also quite well predicted. As an example, in the case of the $4s^2\,^1S_0$ final state the total intensity is slightly overestimated, but all structures seen in the experiment are found from the calculation as well. This good agreement is in clear contrast to the $2p$ Auger decay of Si, where the calculation of the intensities for $3s^2\,^1S_0$ final states failed completely [14].

TABLE III. Experimental and calculated intensity weighted mean kinetic energies and relative intensities of the $M_{4,5}NN$ Auger electron final-state groups of atomic Ge.

	Experiment		Theory	
Assignment	E_k (eV)	Int.	E_k (eV)	Int.
$4s4p\,^1P_1$	3.5	0.10	2.9	0.15
$4s4p\,^3P_{0,1,2}$	6.6	0.76	7.0	0.76
$4s^2\,^1S_0$	15.0	0.14	15.0	0.09

V. CONCLUSIONS

The 3*d* photoionization and subsequent Auger decay of initially neutral atomic Ge have been studied experimentally and theoretically. The experimental spectra were analyzed using multiconfiguration Dirac-Fock calculations that allowed interpretation of the observed spectral features. The 3*d* photoionization binding energies of atomic Ge were provided and the main features of the complete Auger decay spectrum were assigned.

ACKNOWLEDGMENTS

The work has been financially supported by the Research Council for Natural Sciences of the Academy of Finland and the European Community-Research Infrastructure Action under the FP6 "Structuring the European Research Area" Programme (through the Integrated Infrastructure Initiative "Integrating Activity on Synchrotron and Free Electron Laser Science"). S.U. thanks the support from the Finnish Academy under Grant No. 135871 and the Lund University. We are grateful to S. Fritzsche for allowing access to unpublished modules in the RATIP [27] package. We thank also the staff of MAX-lab for their assistance during the experiments.

[1] J. M. Hunter, J. L. Fye, M. F. Jarrold, and J. E. Bower, Phys. Rev. Lett. **73**, 2063 (1994).
[2] J. R. Heath, Y. Liu, S. C. OBrien, Q. L. Zhang, R. F. Curl, F. K. Tittel, and R. E. Smalley, J. Chem. Phys. **83**, 5520 (1985).
[3] Y. Negishi, H. Kawamata, T. Hayase, M. Gomei, R. Kishi, F. Hayakawa, A. Nakajima, and K. Kay, Chem. Phys. Lett. **269**, 199 (1997).
[4] D. Schmeisser, R. D. Schnell, A. Bogen, F. J. Himpsel, D. Rieger, G. Landgren, and J. F. Morar, Surf. Sci. **172**, 455 (1986).
[5] G. Pourtois, M. Houssa, A. Delabie, T. Conard, M. Caymax, M. Meuris, and M. M. Heyns, Appl. Phys. Lett. **92**, 032105 (2008).
[6] T. Hanrath and B. A. Korgel, J. Am. Chem. Soc. **126**, 15466 (2004).
[7] National Institute of Standards and Technology (NIST), Atomic Spectra Database Energy Levels, [http://physics.nist.gov/PhysRefData/ASD/].
[8] K. Tint, A. Kono, and T. Goto, J. Quantum Spectrosc. Radiat. Transf. **43**, 427 (1990).
[9] S. Aksela and H. Aksela, Phys. Rev. A **31**, 1540 (1985).
[10] A. Kovalík, E. A. Yakushev, D. V. Filosofov, V. M. Gorozhankin and Ts. Vylov, J. Electron Spectrosc. Relat. Phenom. **123**, 65 (2002).
[11] R. S. Freund, R. C. Wetzel, R. J. Shul, and T. R. Hayes, Phys. Rev. A **41**, 3575 (1990).
[12] Y.-K. Kim and P. M. Stone, J. Phys. B **40**, 1597 (2007).
[13] K. Jänkälä, S. Fritzsche, M. Huttula, J. Schulz, S. Urpelainen, S. Heinäsmäki, S. Aksela, and H. Aksela, J. Phys. B **40**, 3435 (2007).
[14] K. Jänkälä, S. Urpelainen, M. Huttula, S. Fritzsche, S. Heinäsmäki, S. Aksela, and H. Aksela, Phys. Rev. A **77**, 062504 (2008).
[15] M. Huttula, E. Kukk, S. Heinäsmäki, M. Jurvansuu, S. Fritzsche, H. Aksela, and S. Aksela, Phys. Rev. A **69**, 012702 (2004).
[16] S. Urpelainen, S. Heinäsmäki, M.-H. Mikkelä, M. Huttula, S. Osmekhin, H. Aksela, and S. Aksela, Phys. Rev. A **80**, 012502 (2009).
[17] M. Bässler *et al.*, Nucl. Instr. Meth. Phys. Res. A **469**, 382 (2001).
[18] M. Huttula, K. Jänkälä, A. Mäkinen, H. Aksela, and S. Aksela, New J. Phys. **10**, 013009 (2008).
[19] C. G. King, M. Tronc, F. H. Read, and R. C. Bradford, J. Phys. B **10**, 2479 (1977).
[20] J. Jauhiainen, A. Ausmees, A. Kivimäki, S. J. Osborne, A. Naves de Briton, S. Aksela, S. Svensson, and H. Aksela, J. Electron Spectrosc. Relat. Phenom. **69**, 181 (1994).
[21] F. A. Parpia, C. Froese Fischer, and I. P. Grant, Comput. Phys. Commun. **94**, 249 (1996).
[22] P. Jönsson, X. He, C. Froese Fischer, and I. P. Grant, Comput. Phys. Commun. **177**, 597 (2007).
[23] S. Fritzsche, C. Froese Fischer, and G. Gaigalas, Comput. Phys. Commun. **148**, 103 (2002).
[24] G. Gaigalas, T. Zalandauskas, and S. Fritzsche, Comput. Phys. Commun. **157**, 239 (2004).
[25] A. F. Starace, in *Handbuch der Physik*, edited by W. Mehlhorn (Springer-Verlag, Berlin, 1982), Vol. 1, p. 1.
[26] I. P. Grant, *Relativistic Quantum Theory of Atoms and Molecules* (Springer Science, New York, 2007).
[27] S. Fritzsche, J. Electron Spectrosc. Relat. Phenom. **114**, 1155 (2001).
[28] S. Fritzsche, J. Nikkinen, S.-M. Huttula, H. Aksela, M. Huttula, and S. Aksela, Phys. Rev. A **75**, 012501 (2007).
[29] K. Jänkälä *et al.*, Phys. Rev. A **73**, 022720 (2006).
[30] W. Kutzelnigg and J. D. Morgan, Z. Phys. D **36**, 197 (1996).